Chapter 8

Satellite Climatology of Tropical Cyclone with Concentric Eyewalls

Yi-Ting Yang , Hung-Chi Kuo , Eric A. Hendricks and Melinda S. Peng

Additional information is available at the end of the chapter

http://dx.doi.org/10.5772/64354

Abstract

An objective method is developed to identify concentric eyewalls (CEs) for tropical cyclones (TCs) using passive microwave satellite imagery from 1997 to 2014 in the western North Pacific (WNP) and Atlantic (ATL) basin. There are 91 (33) TCs and 113 (50) cases with CE identified in the WNP (ATL). Three CE structural change types are classified as follows: a CE with the inner eyewall dissipated in an eyewall replacement cycle (ERC, 51 and 56% in the WNP and ATL), a CE with the outer eyewall dissipated first and the no eyewall replacement cycle (NRC, 27 and 29% in the WNP and ATL), and a CE structure that is maintained for an extended period (CEM, 23 and 15% in the WNP and ATL). The moat size and outer eyewall width in the WNP (ATL) basin are approximately 20–50% (15–25%) larger in the CEM cases than that in the ERC and NRC cases. Our analysis suggests that the ERC cases are more likely dominated by the internal dynamics, whereas the NRC cases are heavily influenced by the environment condition, and both the internal and environmental conditions are important in the CEM cases. A good correlation of the annual CE TC number and the Oceanic Niño index is found (0.77) in WNP basin, with most of the CE TCs occurring in the warm episodes. In contrast, the El Niño/Southern Oscillation (ENSO) may not influence on the CE formation in the ATL basin. After the CE formation, however, the unfavorable environment that is created by ENSO may reduce the TC intensity quickly during warm episode. The variabilities of structural changes in the WNP basin are larger than that in the ATL basin.

Keywords: concentric eyewall, microwave satellite, ENSO

1. Introduction

Tropical cyclones (TCs), and particularly strong TCs, are observed with a concentric eyewall (CE) structure that has an inner eyewall and an outer eyewall separated by a convective minimum region [1]. A local tangential wind maximum is associated with the outer eyewall and the most rapid increase in wind speed lies on the inside of the wind maximum [1]. The outer wind maximum thus contracts and intensifies, and then the inner eyewall weakens and eventually vanishes during eyewall replacement cycle (ERC). One of the great challenges associated with TC prediction is the large variability in structure and intensity changes, and the CE formation and the ERC is a mechanism to produce such variability [1–4]. Many theories allude to the influences of both synoptic scale environmental conditions and mesoscale processes in the CE formation. Nong and Emanuel [5] showed that the CE may form due to favorable environmental condition or external forcing and wind-induced surface heat exchange instability. Examples of internal dynamics include propagating vortex Rossby waves (VRWs) that interact with a critical radius [6, 7] and axisymmetrization during a binary vortex interaction [8, 9]. Terwey and Montgomery [10] employed idealized full physics hurricane to demonstrate the secondary eyewall form at region of sufficient low-level radial potential vorticity gradient. The result highlights the VRW energy accumulation in the critical radius with a wind-moisture feedback process at the air-sea interface. Huang et al. [11] suggested that the broadening of the radial tangential wind profile above the boundary layer (BL) in a symmetric fashion can lead to BL convergence and inflow. The progressive strengthening of the BL inflow and the unbalanced BL response may lead to secondary eyewall formation. Previous observational studies indicate that the secondary eyewall can act as a barrier to the moisture inflow to the inner eyewall (e.g., [12]).

Sitkowski et al. [4] used flight-level data to study the ERC process in the Atlantic (ATL) basin. They suggested that large variances are in the ERC time requirement, the intensity, and the change in radii because CEs are not only associated with intensity but also structural changes. Maclay et al. [13] used the low-level area-integrated kinetic energy to show that while the intensity weakens during the ERC, the integrated kinetic energy and the TC size increase. Their results suggest that CE formation and ERC are dominated by internal dynamical processes. The passive microwave data can more clearly reveal the CE structure in TCs. Using microwave data between 1997 and 2002, Hawkins and Helveston [14] suggested that CEs exist with a much higher percentage (80 and 40%) in intense TCs (maximum wind > 120 kts) than previously realized in the western North Pacific (WNP) and ATL basin. As further noted by Hawkins et al. [15], there were more CE cases with large radius in the WNP than in other basins. Hawkins and Helveston [16] provided examples of different modes of CE structure, including the ERC, triple eyewalls [17], ERCs that are repeated multiple times, ERCs that are interrupted by vertical shear and landfall, and cases where an outer eyewall forms at a large radius and remains in a CE structure for a long duration. The different CE modes appear to have profound impacts on intensity and structural forecasts. This study quantitatively examines these structural and intensity changes of CE by an objective method.

There have been extensive studies on TCs in different El Niño/Southern Oscillation (ENSO) phases, and no significant correlation has been found between the annual TC genesis number and ENSO over the WNP basin (e.g., [18]). The annual genesis number, however, increases over the southeastern part of the WNP and decreases over the northwestern part in the El Niño (the warm episode) and a reversed situation occurred in the La Niña (the cold episode) [19, 20]. TCs tend to recurve toward higher latitudes in the periphery of subtropical high system before landfall due to the shift of the genesis region in the warm episode. In contrast, TCs tend to move more westward in the La Niña years ([20], and references therein). The mean duration of TCs over the ocean tends to be longer during the warm episode than that in the cold episode [21]. As a result, there are more intense and long-lived typhoons in the warm episode than in the cold episode [19, 22]. In the ATL basin, ENSO inhibits the formation of TCs through the enhancement of the vertical wind shear, subsidence, and reduced relative humidity in the tropical ATL [20, 23, 24]. Teleconnection theory suggests that warm-free tropospheric temperatures that are spread eastward from the Pacific by equatorial wave dynamics can be unfavorable to convection and can influence sea surface temperature (SST) in the ATL ([25], and references therein). As stated above, shifts in TC tracks and environmental conditions have been linked to phase changes in ENSO. Since the variations in the environment have been linked to CE characteristics [26], we examine frequency and storm structures of CE TCs in relation to ENSO.

In this chapter, we present the data, the objective CE identification method, and the CE structural and intensity changes in the WNP and ATL basins. The relationship between CE TCs and ENSO is discussed and a conclusion is presented at the end of the chapter.

2. Data and methodology

The passive Special Sensor Microwave/Imager (SSM/I) 85 GHz horizontal polarized orbital imagery and Tropical Rainfall Measuring Mission (TRMM) Microwave Imager (TMI) data from the polar-orbiting TRMM satellite [27] are used in this study. These data were obtained from the website of Naval Research Laboratory (NRL) Marine Meteorology Division [15, 28]. The microwave satellite images are available and online since 1997, and the TRMM satellite ended collecting data from April 15, 2015. We use the microwave satellite data to examine the characteristics of TCs with CEs in the WNP and ATL basins between 1997 and 2014 for consistent data. The National Centers for Environmental Prediction (NCEP) warm and cold episode data are based on a threshold of ±0.5°C for the Oceanic Niño Index (ONI) in the Niño 3.4 region (5°N-5°S, 120°170°W). The ONI data are a product of three-month time running mean of SST in the Niño 3.4 region and they are used to classify the environmental condition of CE formation. The Niño 3.4 SST anomaly is used because it is better correlated with overall tropical storm activity [21].

The microwave satellite images are reprocessed using the Backus-Gilbert theory of reference [29] to create high-resolution (1–2 km) products that can assist in defining inner storm structural details [14, 15]. These images are stored as 800 × 800 pixel color jpeg files that are

composed with red (R), green (G), and blue (B) colors. The pixels of R, G, and B components are converted into the high-resolution brightness temperature (T_B) based on the color table in the picture. To identify CE typhoons, the T_B dataset is transformed from Cartesian to polar coordinates with the TC center as the origin. The TC center is determined based on the Joint Typhoon Warning Center (JTWC) best track data at the time closest to satellite observation as the TC center. To further smooth the data and also to be consistent with the center position uncertainty of 10 km, we employ 5 pixel averages in the radial direction and a 45-degree sector average of T_B to obtain eight radial profiles for the bin data. In each bin of the radial profile, the T_B mean value and the standard deviation (σ) within each 45-degree sector were calculated. An objective method is developed to identify the CE structure from the eight radial profiles. The method involves the following five sequential steps:

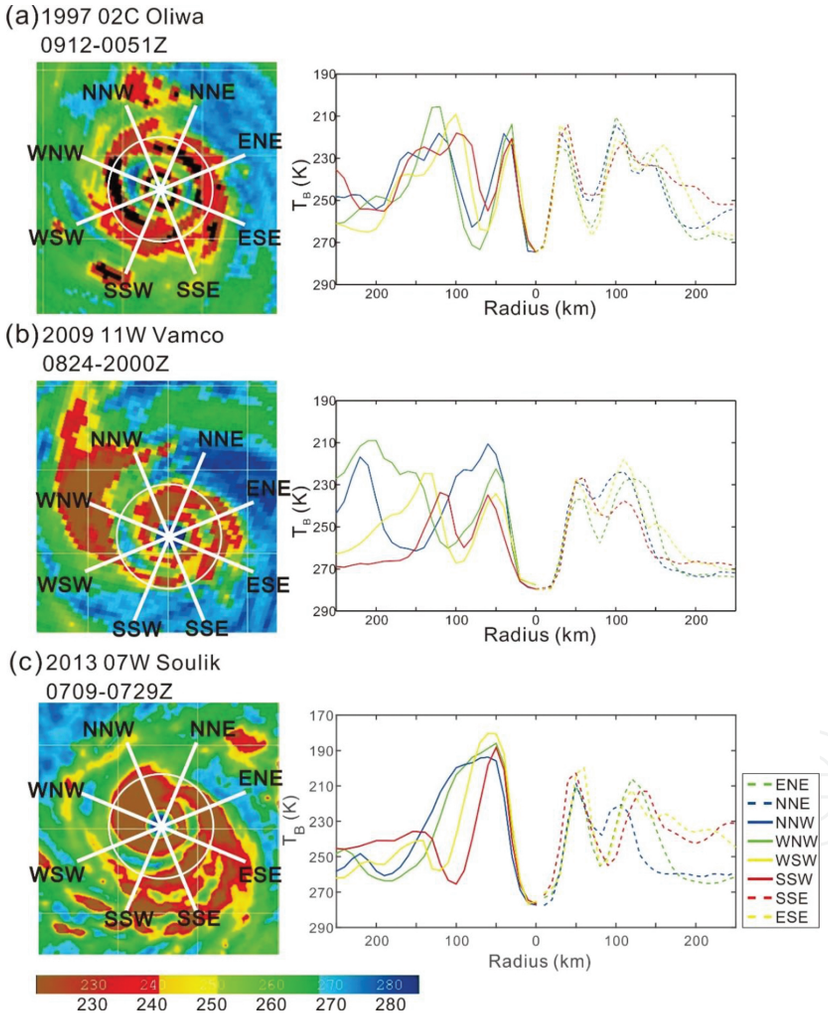

Figure 1. Color-enhanced microwave CE imageries of typhoons (a) Oliwa (1997), (b) Vamco (2009), and (c) Soulik (2013). The averaged T_B profiles of eight radial directions for Typhoon Oliwa are conformed to the CE-determined criteria. The secondary T_B minimum for Typhoon Vamco only identified spiral outer rainband. One-half symmetry of Typhoon Soulik identified CE structure (solid green: WNW; solid yellow: WSW; solid red: SSW; solid blue: NNW; dash green: ENE; dash yellow: ESE; dash red: SSE; and dash blue: NNE). Figures (a) and (b) from Yang et al. [26], courtesy of American Meteorological Society.

http://dx.doi.org/10.5772/64354

1. Within 150 km distance of the TC center, check for the existence of one local maximum T_B between two minimum T_B in each profile.
2. Check in each profile that the local T_B maximum and minimum satisfy the criteria of $T_{Bmax} \geqq \sigma_{outer\_min} + T_{Bouter\_min}$ and $T_{Bmax} \geqq \sigma_{inner\_min} + T_{Binner\_min}$.
3. For the profiles that satisfy criteria (1) and (2), check if $T_{Bouter\_min} \leqq 230K$.
4. Check if at least five out of eight sectors satisfy the above three criteria.
5. Check if the radial distance between any sectors of the two outer eyewalls is smaller than 50 km.

	Satisfy criteria (1)–(5)	**Satisfy criteria (1)–(5) but criterion (3): $T_{Bouter—min}$**		**Satisfy criteria (1)–(5) but criterion (4):**		**No criterion (5)**
		≤220K	**≤240K**	**≥6/8 sectors**	**≥4/8 sectors**	
WNP	113	89	130	76	145	124
ATL	50	37	60	33	64	58

Table 1. The numbers of CE cases when we use criterion (3) by making outer eyewall convection criterion 10 K weaker and stronger (240 and 220 K) than 230 K, use criterion (4) by making 4/8 and 6/8 symmetry to identified CE structure, and do not use criterion (5).

Criterion (1) identifies the existence of the structure that resembles the moat and the double eyewall in each of the eight radial profiles. Criterion (2) ensures that the moat is significant and criterion (3) ensures that the outer eyewall has strong convection. Criterion (4) ensures axisymmetry of double eyewall structure and criterion (5) ensures that the outer eyewall identified is not a spiral band. **Figure 1** provides an example of the CE TC and the no-CE TC and their associated T_B radial profiles. Three examples that have the T_B profiles of two local minima (double eyewalls) and one maximum in between the minima (the moat) are presented in **Figure 1**. The no-CE Typhoon Vamco (2009) is not classified as a CE typhoon based on our criterion (5), with the convection in the outer eyewall identified as a spiral band. Compare with CE Typhoon Oliwa (1997), Typhoon Soulik (2013) is not classified as a CE typhoon at this time based on criteria (3) and (4). If we relax criterion (3) from 230 to 240 K, or relax criterion (4) from five to four out of eight sectors, it can be considered a CE typhoon. The objective method allows us to systematically identify CE typhoons from dataset. We examined 29,785 (19,001) SSM/I and TMI satellite images in the WNP (ATL) basin from the NRL website. Out of these, 113 (50) CE cases were identified, including 17 (11) cases of multiple CE formation. There are 91 (33) CE typhoons identified in the WNP (ATL) basin. **Table 1** shows the numbers of CE cases with sensitivities in criterion (3) by making outer eyewall convection 10 K weaker and stronger (240 and 220 K) than 230 K, in criterion (4) by making 4/8 and 6/8 symmetry, and no criterion (5). Consistent with the subjective work of Kuo et al. [3], the five criteria of reference [26] ensure that the CE typhoons identified are axisymmetric with a significant moat and a strong outer eyewall while retaining enough cases for statistics. The inner eyewall radius was determined as the distance be-

tween the typhoon center to the point where $T_B = 0.5 \times \sigma_{inner} + T_{Binner}$. The moat width was determined by the distance between the points of $T_B \geqq 0.5 \times \sigma_{outer} + T_{Bouter}$ and $T_B \geqq 0.5 \times \sigma_{inner} + T_{Binner}$. Finally, the outer eyewall width was determined by the distance of the region that satisfies $T_B < 0.5 \times \sigma_{outer} + T_{Bouter}$ in the outer eyewall region. The inner eyewall radius, the moat, and the outer eyewall width were calculated by averaging the radial profiles of the eight sections as shown in **Figure 1**.

3. Structural and intensity change of concentric eyewall

In order to study the structural and intensity changes of CE TCs, we excluded the case when the TC's outer eyewall was within 200 km from land in the period of 24 h before and after CE formation, or where the satellite temporal resolution was greater than 12 h in the WNP (ATL) basin. There were 83 and 34 CE cases analyzed in the WNP and ATL basins, respectively. Three different structural change processes were defined after CE formation. The eyewall replacement cycle (ERC) cases were classified based upon the dissipation of the inner eyewall in less than 20 h after CE formation. The cases in which part of the outer eyewall dissipates within 20 h are classified as no replacement cycle (NRC) cases. The cases where the CE structure is maintained for more than 20 h are classified as concentric eyewall maintained (CEM) cases. The similar inner core size requirement was used to avoid assigning a CE TC with multiple ERC processes into one single CEM case.

The ERC classification had 42 of 83 cases and 19 of 34 cases (51 and 56%) in the WNP and ATL basins, respectively. The CEM classification had 19 and 5 cases (23 and 15%) in the WNP and ATL basins, respectively. The NRC classification had 22 and 10 cases (27 and 29%). Examples of the three classifications for the CE processes are shown in **Figure 2**. The NRC cases resemble "the shear stop ERC mode" and the CEM cases "the large radius outer eyewall and CE structure maintained for a time cases" as discussed in the study of Hawkins and Helveston [16].

Figure 3a and **b** shows the composite time series of intensities for the ERC, CEM, NRC cases as well as the average of the total CE sample. In the WNP basin, the average intensity of CEM cases is stronger than that of the ERC and NRC cases before and after CE formation. In particular, the CEM storms intensified continuously for 18 h after CE formation and maintained the intensity for another 24 h. The composite intensity of ERC and NRC cases is similar to that before CE formation. In the ATL basin, although the composite intensity of ERC is stronger than that of CEM continuously for 18 h before CE formation and 36 h after CE formation, the CEM cases maintained similar intensity before CE formation. Furthermore, the intensity of NRC decreases quickly after CE formation in both basins. **Figure 3a** and **b** indicates that a key feature of CE formation appears to be the maintenance of a relatively high intensity for a longer duration rather than a rapid intensification process to a high intensity. The stronger core intensity may play a pivotal role in the axisymmetrization dynamics of asymmetric convection outside the core to produce the CE structure [8, 9]. This asymmetric convection is also shown in **Figure 2**.

http://dx.doi.org/10.5772/64354

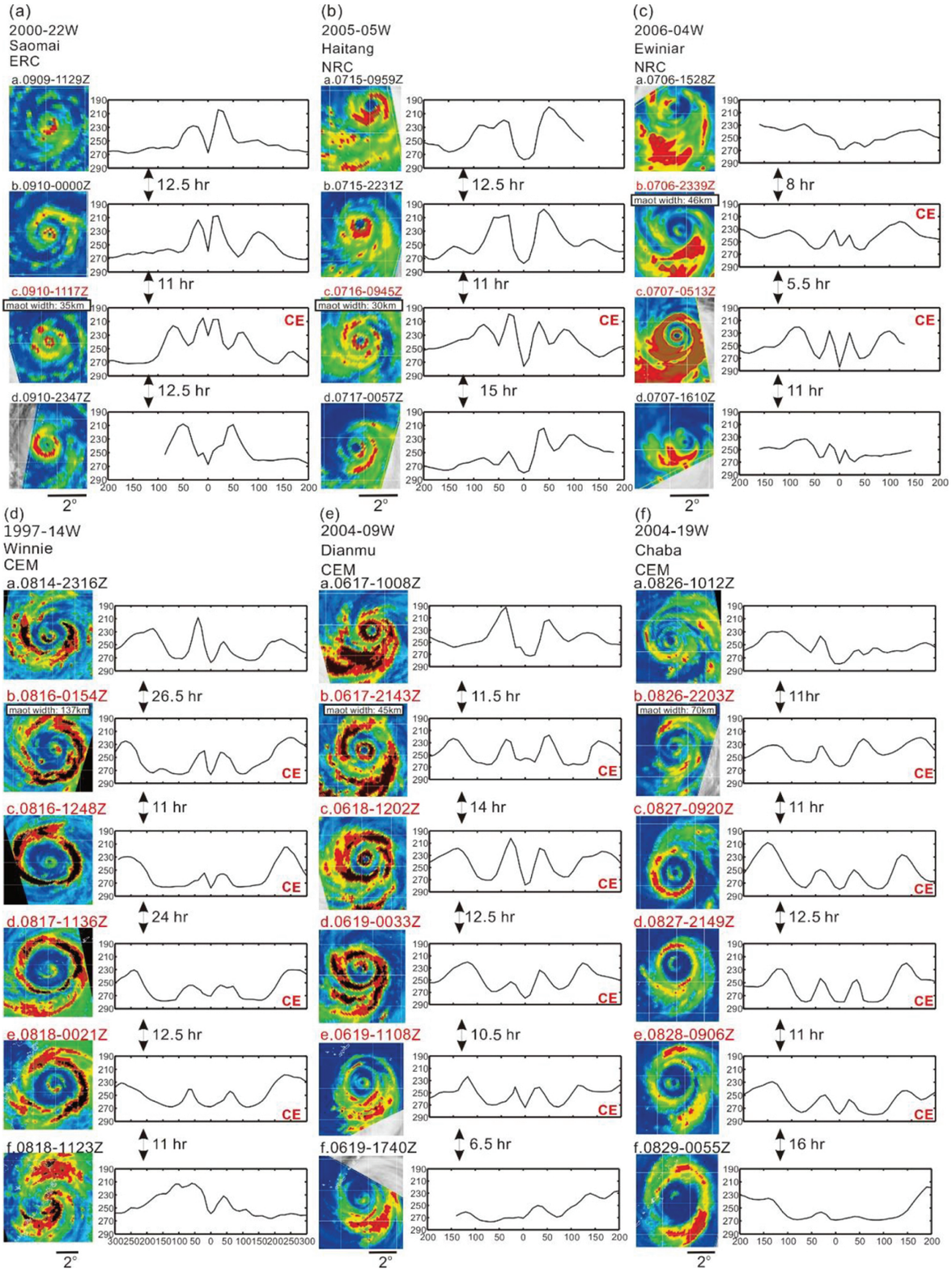

Figure 2. The imagery sequences and averaged TB radial profile for (a) Typhoon Saomai 2000-ERC, (b) Haitang 2005-NRC, (c) Ewiniar 2006-NRC, (d) Winnie 1997-CEM, (e) Dianmu 2004-CEM, and (f) Chaba 2004-CEM. From Yang et al. [26], courtesy of American Meteorological Society.

Maclay et al. [13] use aircraft data to construct the K-V_{max} diagram for the intensity and structural changes. However, there is few active aircraft reconnaissance program for the WNP basin. Therefore, the structural and intensity variability is illustrated here using the T-V_{max} diagram (where T is the T_B and V_{max} is the best track estimated intensity). The convective activity (CA) is indicated by the areal averaged T_B contrast to the background T_B in the 400 km square area of satellite imagery centered at the eye ($CA \equiv -\overline{T_{B1} - T_{B0}}$). The background T_{B0} is calculated as the highest 5% of T_B in the 400 km square area. The 400 km square box in general is sufficient to cover the structure of CE TCs.[1] Yang et al. [30] also used T-V_{max} diagram to analyze Typhoon Soulik (2013), which had two long-lived CE episodes. **Figure 3c** and **d** shows the T-V_{max} diagrams for average values of intensity and CA for the no-CE TCs with intensity category 4 or above and far from land (NCE), and CE TCs. The CE cases have stronger averaged CA, in particular, the CEM cases indicates significant CA increase 24 h after CE formation in the WNP basin. The maintenance or a slight increase of the CA for three types and a slower decrease than that of NCE cases in both basins are in general agreement with the notion that the CE TCs can lead to storm growth [13]. The decrease of areal averaged T_B and the increase of kinetic energy both occurred after the ERC process.

Figure 3e and **f** indicates that the outer eyewall width is larger with a larger moat width (R^2 = 0.5) in both basins. All the CEM cases have moat widths greater than 30 km in both basins. In particular, the CEM cases on average have slightly higher intensities, larger moat widths, and larger outer eyewall widths than those of ERC and NRC cases. The CEM cases in the ATL basin also have similar characteristics except the average intensity slightly lower than that of ERC. The ATL basin is smaller than WNP basin, only five CEM cases are classified in the ATL basin. If we choose 15 h (10 h) for CEM criteria, eight (18) cases are classified into CEM cases in the ATL basin. These CEM cases on average have higher intensity, larger moat widths, and larger outer eyewall widths. In general, the moat size and outer eyewall width are approximately 20–50% (15–25%) larger in the CEM cases than that in the ERC and NRC cases. The very large moat and outer eyewall width in the CEM cases may have some implications for the long duration of CE structure. Willoughby [31] presented a scale analysis on the validity of the balance model and the transverse circulation equation in the TC. Rozoff et al. [32] used the balanced model transverse circulation equation to study the ERC dynamics. In this manner, the balance dynamics of the CE is scale free, namely, the dynamics may occur in different scales where the balance equation assumption is valid. Thus, it is possible that the larger CE storms simply end up taking much longer time to contract due to their larger scale. Rozoff et al. [32] showed that the decay of the inner eyewall may be related to the fact that the upper warm core has a larger stabilization effect on the convection in the inner eyewall than it does on the convection in the outer eyewall. The stabilization effect of upper warm core argument cannot explain why the inner eyewall is maintained for such a long time in the CEM cases. We also note that the CE variabilities of intensity and structural changes in the WNP basin are larger than that in the ATL basin as shown in **Figure 3**.

1 Typhoons Winnie (1997) and Amber (1997) were very large, and these quantities are calculated using a 600 km square box.

http://dx.doi.org/10.5772/64354

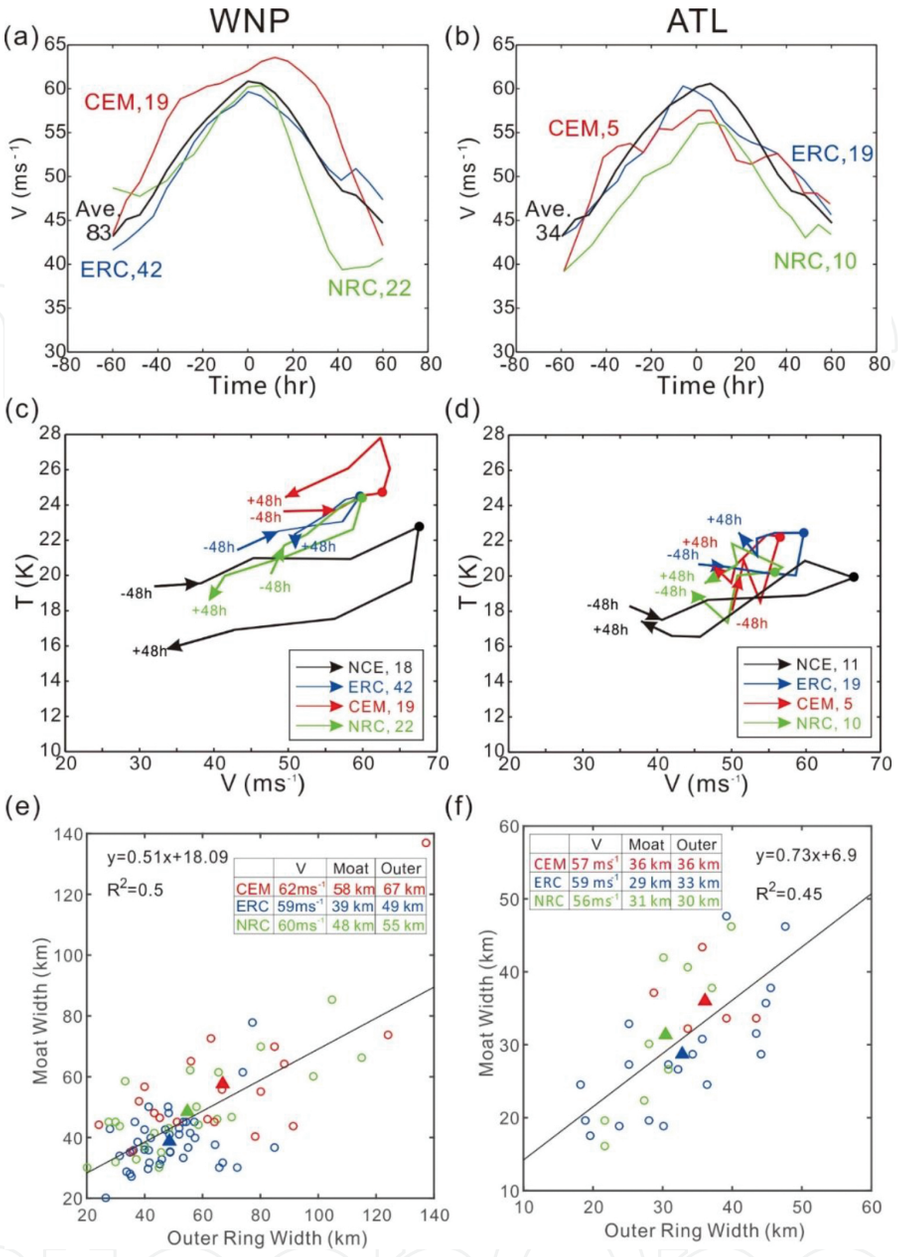

Figure 3. (a and b) Composite time series of intensity for the ERC, CEM, NRC cases, and the all CE cases in WNP and ATL basins. (c and d) The averaged T_B and intensity changes in 48 h before and after the peak intensity/CE formation for the NCE, ERC, CEM, and NRC cases in WNP and ATL basins. Case numbers are given. The dots are CE formation time for CE cases and V_{max} time for NCE cases. (e and f) Scatter diagrams of the moat width versus outer eyewall width in the WNP and ATL basins. The linear fitting line and formula are also shown. The table indicates the average intensity, moat width, and outer eyewall width of CEM, ERC, and NRC cases, respectively.

On the other hand, the occurrence of barotropic instability will invalidate the axisymmetric balance assumption. Kossin et al. [33] identified two types of barotropic instabilities in the vorticity field with CE structure: the instabilities across the outer eyewall (Type I) and across the moat (Type II) due to the sign reversal of the radial vorticity gradient. These instabilities may work against the maintenance of the CE structure. The large moat size in the CEM cases has two dynamic implications. It reduces the growth rate of the Type II instability across the

moat which is favorable for the CE structure maintenance; and it also lessens the stabilization of the core vortex on the Type I instability across the outer eyewall which is not favorable for the CE maintenance. As demonstrated by Kossin et al. [33], the thicker outer eyewall is more stable for the type I instability, which is favorable for maintaining the outer eyewall structure. These observations of the large outer eyewall and moat widths are in general agreement with the concept that barotropic dynamics may play a significant role in maintaining the CE structure for CEM cases.

Finally, we note that the large moat size in the CEM cases may have an impact on the convection and subsidence in both eyewalls. The interference between the convection/subsidence couplet of the inner and outer eyewalls may be reduced when the moat size is very large. The large moat size may assist the inner core by suppressing potentially competing convection while the subsidence concentrated radial outward may make it less likely to penetrate to the eyewall. Zhou and Wang [34], in the modeling study, revealed that the demise of the inner eyewall is primarily due to the interception of the BL inflow supply of entropy by the outer eyewall. The interception process becomes inefficient when the moat size is large. **Figure 3e** and **f** suggests that the internal structure of CE TCs, such as the general high intensity with the large widths of the moat and outer eyewall, may be important for the maintenance of the CE structure in the CEM cases.

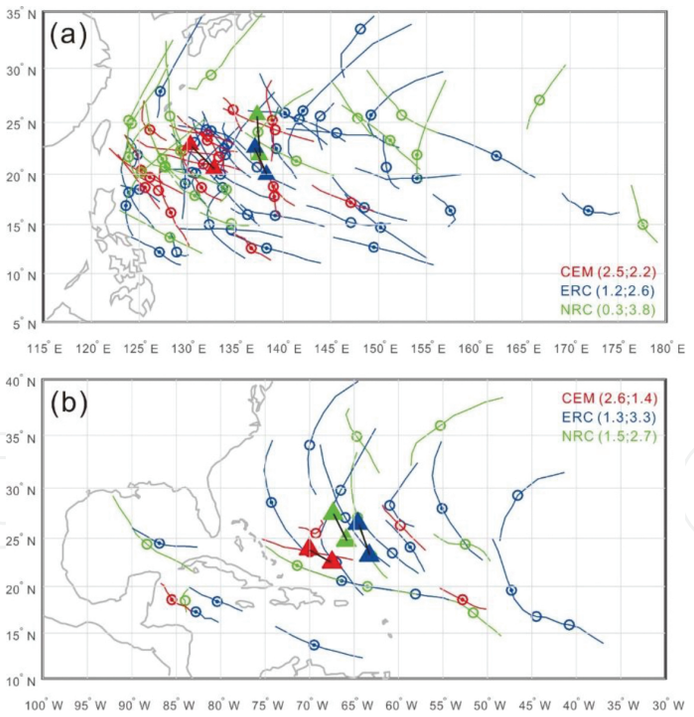

Figure 4. (a) Tracks within 48 h centered at CE formation in the WNP. The ERC, NRC, and CEM cases are represented by blue, green, and red colors, respectively. The circles with (without) a dot are the location of the secondary eyewall formation with intensity greater than or equal to (less than) category 4 on the Saffir-Simpson scale. The triangle symbols represent the composite location of CE formation and 24 h after CE formation. The average translation speed of zonal and meridional between CE formation and 24 h after CE formation is shown. (b) As in (a) but the cases in the ATL basin.

http://dx.doi.org/10.5772/64354

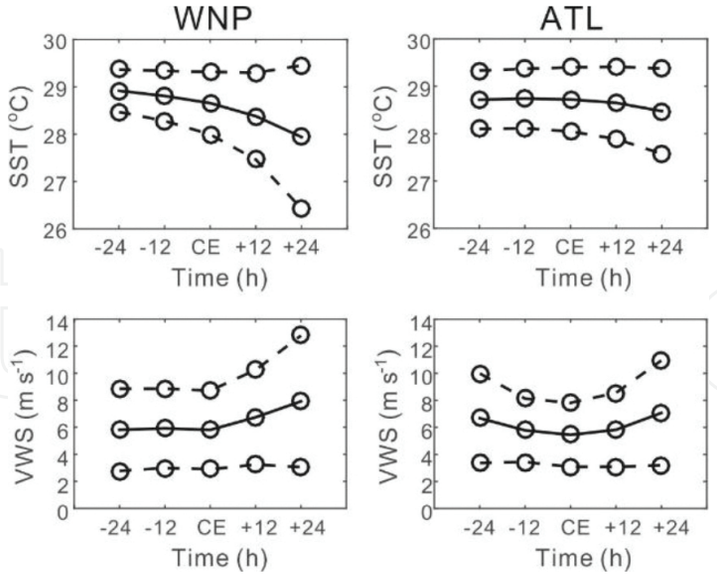

Figure 5. The time series of SST and 850–200 mb vertical shear (VWS) in the WNP and ATL basins. The solid lines mean average value. The dash lines mean average value ± 1 standard deviation.

Figure 4a shows the locations of CE formation on the tracks 24 h before and after the formation. Most CEM cases are located west of 140°E with the smallest northward translation speed of 2.2 m s^{-1} in the WNP basin. This suggests TCs tend to be more intense in the western part of Pacific after a long journey over ocean. In the ATL basin, the average location of CEM cases is farther west than that of ERC and NRC cases with the smallest northward translation speed of 1.4 m s^{-1}. Compared with ERC and NRC cases, CEM cases encounter warmer SST after CE formation. On the other hand, the NRC cases have a larger northward translation speed (3.8 m s^{-1}) in the WNP basin, and the average location of CE formation is farther north (25°N) than that of ERC and CEM cases in the ATL basin. The composite time series with respect to CE formation time for SST, relative humidity (RH), ocean heat content (OHC), and maximum potential intensity (MPI) decrease and vertical shear increases with time because TCs in general move toward the northwest direction by the Statistical Typhoon/Hurricane Intensity Prediction Scheme model data (STIPS/SHIPS; [35, 36]). The large northern translation speed of the NRC cases causes them to experience colder SST, larger vertical wind shear, smaller RH, smaller OHC, and smaller MPI 24 h after CE formation (not shown; the result of WNP cases is presented in **Figure 10** of reference [26]). These phenomena are consistent with the sharp decrease of CA and intensity in NRC cases as shown in **Figure 3**. The dissipation of the outer eyewall in the NRC cases presumably may also be related to the strong vertical shear in the high latitudes [16]. Moreover, the CEM cases were under small vertical wind shear, high SST, OHC and MPI, and high low- to mid-level RH throughout the period of CE formation. These favorable environment factors may help CEM cases maintain their intensity and eyewall structures. The environmental conditions play a role in the structural and intensity changes of CEM and NRC TCs. **Figure 5** shows that the variabilities of SST and 850–200 mb vertical wind shear during CE formation and after CE formation are larger in the WNP basin than that in the ATL basin. This results in the larger CE variabilities of intensity and structural changes in the WNP basin (**Figure 3**).

4. The relationship between CE TC and ENSO

The environmental factors and TC activities are deeply affected by ENSO and have been examined by many previous studies. We have discussed the importance of environmental factors for CE TCs in Section 3. In this section, we followed Yang et al. [38] but included CE cases in the ATL basin. Furthermore, we examined the CE TCs in different phases of ENSO. There are 46 months for five warm episodes, 62 months for four cold episodes, and 103 months for eight neutral episodes during 1997–2014 period according to NCEP data. There are 38 (18), 16 (10), and 59 (22) CE TCs occurred in the warm, cold, and neutral episodes in the WNP (ATL) basin.

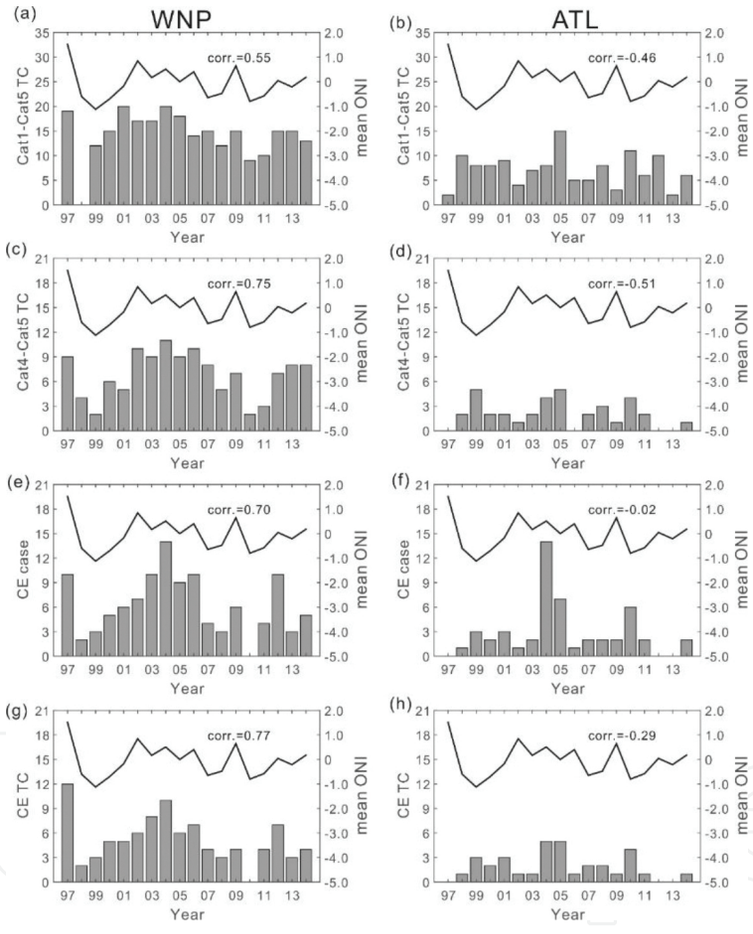

Figure 6. Number of (a) category 1–5 TCs, (c) category 4–5 TCs, (e) CE cases (multiple CE formations are included), and (f) CE TCs by years (histograms and left ordinate) and the mean ONI by year (line and right ordinate) in the WNP basin. The correlation between number and mean ONI is shown. (b, d, f, and h) As in (a, c, e, and h) but in the ATL basin.

In the WNP basin, the correlation between annual CE TCs number (CE cases) and ONI by year is 0.77 (0.70) as shown in **Figure 6**. **Figure 6** also shows that the correlation between ONI and annual strong TCs of Category 4 or stronger is 0.75, which means more intense TCs occur in the El Niño phase than that in the La Niña phase. This is in general agreement with previous

studies [19, 22]. All the CE-related correlations are higher than the correlation of TC number and ONI by year (0.55). The better correlation of CE TCs and ONI may be due to the fact that the CE structure is likely to occur in strong TCs [3]. In the ATL basin, the negative correlation of annual TCs (strong TCs) and ONI is −0.46 (−0.51), which is consistent with previous studies [20, 23, 24, 37] that suggest unfavorable environment for TC formation in the El Niño phase. Moreover, the worse negative correlation of CE TCs and ONI may be because of only 33 CE TCs in the ATL basin. In addition, the better correlation with CE TCs than with CE cases may be due to the fact that multiple CE formation may be controlled by both internal and environmental factors in both basins.

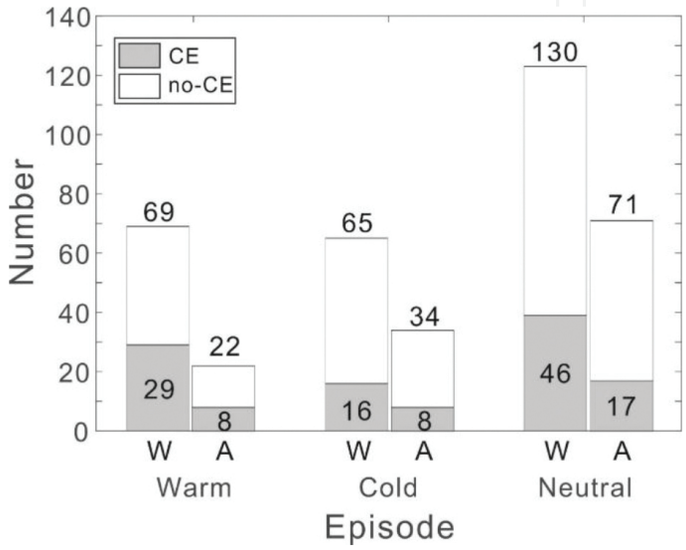

Figure 7. Histogram of the no-CE TCs and CE TCs in three different episodes. The numbers of total TC and CE TCs in each episode are indicated. The letters W and A mean WNP and ATL basin, respectively.

Figure 7 indicates that 42% (35%) of TCs possessed CE structures in their lifetimes during warm (neutral) episodes in the WNP basin. In contrast, only 25% of TCs formed CE structure in the cold episodes. In the ATL basin, 36% (approximately 24%) of TCs possessed CE structures in their lifetimes during warm (neutral and cold) episodes. Moreover, **Table 2** shows that there are 1.5 (0.5), 1.3 (0.7), and 1.0 (0.5) TC formations per month in the WNP (ATL) basin during warm, neutral, and cold episodes, respectively. The monthly CE formation frequencies are 0.8 (0.4), 0.6 (0.2), and 0.3 (0.2) in the WNP (ATL) basin during warm, neutral, and cold episodes, respectively. **Figures 6** and **7** and **Table 2** suggest that ENSO may create a better environment for CE formation in the WNP basin. In the ATL basin, the slightly higher monthly CE formation frequency during warm episode may be due to the farther south CE location as shown in **Figure 8**. For the WNP basin, **Figure 8a** suggests that CE cases during cold (warm) episodes tend to occur farther west (east). The eastward shift of the genesis region may be due to the warm sea water and moist air extending farther east (west) over the WNP during warm (cold) episodes, and the weak vertical wind shear in the southeast part of WNP during warm episodes. This result is consistent with the eastward shift of the TC genesis region in the warm episode [19, 20]. For the ATL basin, **Figure 8b** shows that the average location of CE formation

during warm and cold episodes is similar. After 24 h of CE formation, however, the 850–200mb vertical wind shear in the cold episode is 2–6 m s^{-1} weaker than that in other episodes (not shown) and may help in CE maintenance. The farther south CE location during warm episode may lead to the slight CE formation frequency.

	Warm	Cold	Neutral
WNP TC number/month	69/46 = 1.5	65/62 = 1.0	130/103 = 1.3
WNP CE cases/month	38/46 = 0.8	16/62 = 0.3	59/103 = 0.6
ATL TC number/month	22/46 = 0.5	34/62 = 0.5	71/103 = 0.7
ATL CE cases/month	18/46 = 0.4	10/62 = 0.2	22/103 = 0.2

Table 2. The number of TCs, CE cases, and multiple CE cases per month during warm, cold, and neutral episodes.

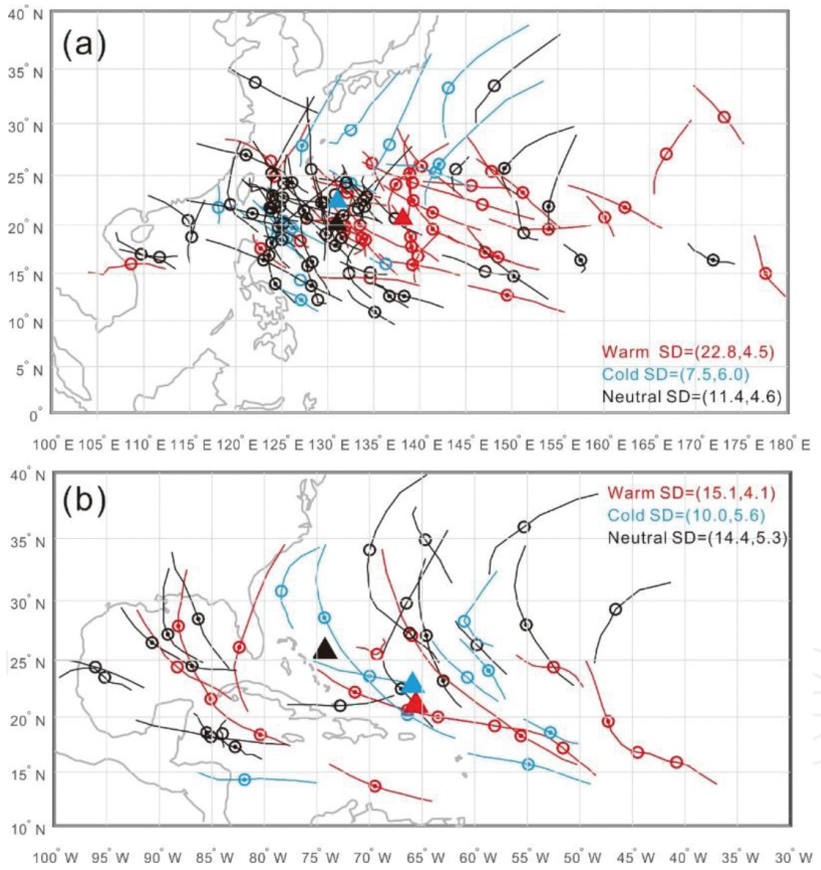

Figure 8. Same as **Figure 4** but during warm (red), cold (blue), and neutral (black) episodes. The triangle symbols represent the composite location of CE formation. The standard deviations of zonal and meridional locations are shown.

Figure 9 suggests that there are only three CEM cases during cold episode in the WNP basin. In addition, there are 12% (3%) of CE cases with more than 30 h long duration in the WNP (ATL) basin. The CE storms in the cold episode have a more rapid intensification rate than that of the warm episode before the CE formation (**Figure 10**). Specifically, there are 13 out of 16

storms in cold episode with intensity change which meet the rapidly intensifying criteria of $\Delta V_{max} \geq 19.5$ m s^{-1} in 24 h [39]. The storm intensity change after the CE formation during warm (cold) episodes often decreases slowly (quickly). The quick decline of intensity during cold episodes may be due to the encountering of unfavorable environmental factors such as the colder SST. **Figure 10b** indicates the similar trends of the average intensity before CE formation in the ATL basin. However, a rapid decreasing trend 24 h after CE formation is in the warm episode. In summary, the CE formation in the ATL basin may not be affected by ENSO because of the average location of CE formation during warm episode farther south over the ATL. After CE formation, the unfavorable environment which is created by ENSO may reduce the TC intensity quickly during warm episode.

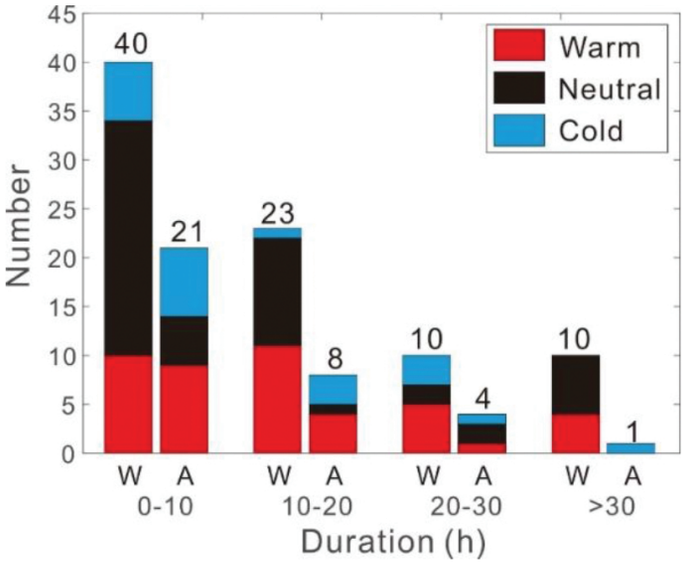

Figure 9. The number of CE cases in different episodes as a function of duration time. The letters W and A mean the WNP and ATL basins, respectively.

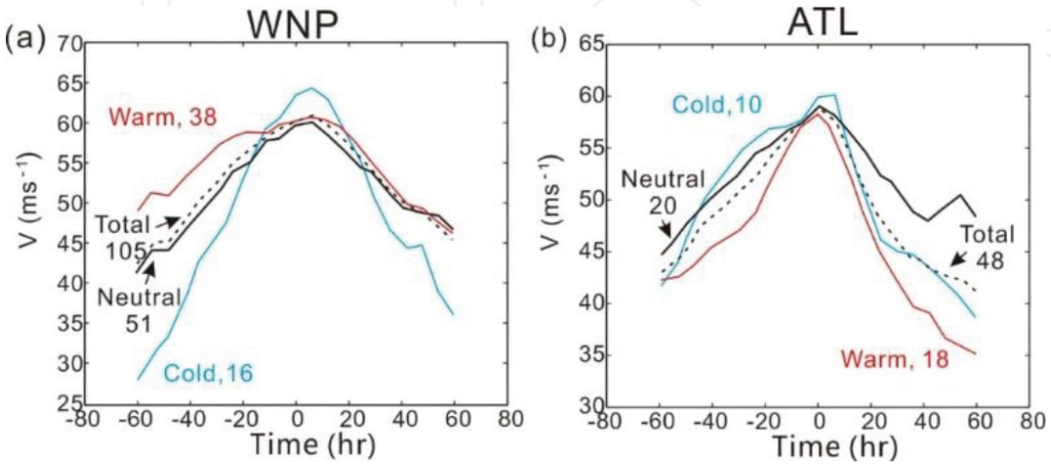

Figure 10. Same as **Figure 3** but during warm, cold, and neutral episodes and all CE cases.

5. Summary and conclusions

An objective method is developed to categorize concentric eyewall structures in the western North Pacific (WNP) TCs using the NRL SSM/I and TMI satellite imagery database. For the WNP (ATL) basin, there are 91 (33) CE TCs and 113 (50) CE cases identified from 29,785 (19,001) satellite images between 1997 and 2014. Excluding the cases that are 200 km close to landfall and cases with temporal resolution higher than12 h, 83 (34) CE cases were studied for the structural and intensity changes. The primary findings are as follows:

1. Three CE types are categorized: CE with an eyewall replacement cycle (ERC; 51 and 56% in the WNP and ATL), CE with no replacement cycle (NRC; 27 and 29% in the WNP and ATL), and CE that is maintained for an extended period of time (CEM; 23 and 15% in the WNP and ATL). The mean duration of CEM type is 32 and 27 h in the WNP and ATL basins, respectively.

2. The CEM cases have relatively high intensity, large widths of both the moat and outer eyewall that last for a long duration time. The large widths of the moat and outer eyewall may reduce the barotropic instabilities of CE storms and thus maintain the CE structures for a long time.

3. Most CEM cases in the WNP basin are located to the west of 140°E with the smallest northward translation speed of 2.2 m s^{-1}. The average location of CEM cases in the ATL basin is farther west than that of ERC and NRC cases with the smallest northward translation speed of 1.4 m s^{-1}. The NRC cases often have fast northward translation speeds and are located in higher latitudes of relative strong vertical shear and cold SST zones. The unfavorable environmental conditions thus act to weaken the convective activity for these cases. On the other hand, the CEM cases occur in favorable environment and tend to form in the warm episode of ENSO in the WNP basin. There are 12% (3%) of CE cases with more than 30 h long duration in the WNP (ATL) basin.

4. The variabilities of intensity and structural changes in the WNP basin are larger than that in the ATL basin. For example, the moat size and outer eyewall width in the WNP (ATL) basin are approximately 20–50% (15–25%) larger in the CEM cases than that in the ERC and NRC cases.

5. In the WNP basin, a very good relationship of 0.77 was found between the annual CE TC numbers and the NCEP Oceanic Niño Index (ONI). The probability of CE TCs formation is strongly influenced by the ENSO environmental factors. For example, there are 29 out of 69 (42%) TCs that possess CE structures in the warm episode. In contrast, there are only 16 out of 65 (25%) TCs that possess CE structures in the cold episode. The averaged CE formation frequencies are 0.8 and 0.3 per month in the warm and cold episodes, respectively.

6. In the ATL basin, the correlation between ONI and CE formation frequency suggests that the ENSO may not influence the CE formation. It may be due to the average location of CE formation during warm episode farther south over the ATL in the relative warm SST

region. After CE formation, however, the unfavorable environment that is created by ENSO may reduce the TC intensity quickly.

Acknowledgements

This work was supported by the Ministry of Science and Technology in Taiwan under grants MOST 104-2111-M-002-002-MY3 and MOST 104-2625-M-002-006, and the Naval Research Laboratory under grant N62909-15-1-2008.

Author details

Yi-Ting Yang[1], Hung-Chi Kuo[2*], Eric A. Hendricks[3] and Melinda S. Peng[4]

*Address all correspondence to: kuo@as.ntu.edu.tw

1 Taida Institute for Mathematical Sciences, National Taiwan University, Taipei, Taiwan

2 Department of Atmospheric Sciences, National Taiwan University, Taipei, Taiwan

3 Department of Meteorology, Naval Postgraduate School, Monterey, California, USA

4 Marine Meteorology Division, Naval Research Laboratory, Monterey, California, USA

References

[1] Willoughby, H. E., J. A. Clos, and M. G. Shoreibah, 1982: Concentric eye walls, secondary wind maxima, and the evolution of the hurricane vortex. J. Atmos. Sci., 39, 395–411.

[2] Black, M. L., and H. E. Willoughby, 1992: The concentric eyewall cycle of Hurricane Gilbert. Mon. Wea. Rev., 120, 947–957.

[3] Kuo, H.-C., C.-P. Chang, Y.-T.Yang, and H.-J. Jiang, 2009: Western North Pacific typhoons with concentric eyewalls. Mon. Wea. Rev., 137, 3758–3770.

[4] Sitkowski, M., J. P. Kossin, and C. M. Rozoff, 2011: Intensity and structure changes during hurricane eyewall replacement cycles. Mon. Wea. Rev., 139, 3829–3847.

[5] Nong, S., and K. A. Emanuel, 2003: A numerical study of the genesis of concentric eyewalls in hurricane. Quart. J. R. Meteor. Soc., 129, 3323–3338.

[6] Montgomery, M. T., and R. J. Kallenbach, 1997:Atheory for vortex Rossby-waves and its application to spiral bands and intensity changes in hurricane. Quart. J. R. Meteor. Soc., 123, 435–465.

[7] Peng, J., T. Li, and M. S. Peng, 2009: Formation of tropical cyclone concentric eyewalls by wave-mean flow interactions. Adv. Geosci., 10, 57–71.

[8] Kuo, H.-C., L.-Y. Lin, C.-P. Chang, and R. T. Williams, 2004: The formation of concentric vorticity structures in typhoons. J. Atmos. Sci., 61, 2722–2734.

[9] Kuo, H.-C., W. H. Schubert, C.-L. Tsai, and Y.-F. Kuo, 2008: Vortex interactions and barotropic aspects of concentric eyewall formation. Mon. Wea. Rev., 136, 5183–5198.

[10] Terwey, W. D., and M. T. Montgomery, 2008: Secondary eyewall formation in two idealized, full-physics modeled hurricanes. J. Geophys. Res., 113, D12112.

[11] Huang, Y.-H., M.-T. Montgomery, and C.-C. Wu, 2012: Concentric eyewall formation in Typhoon Sinlaku (2008). Part II: Axisymmetric dynamical processes. J. Atmos. Sci., 69, 662–674.

[12] Barnes, G. M., and M. D. Powell, 1995: Evolution of the inflow boundary layer of Hurricane Gilbert (1988). Mon. Wea. Rev., 123, 2348–2368.

[13] Maclay, K. S., M. DeMaria, and T. H. Vonder Haar, 2008: Tropical cyclone inner-core kinetic energy evolution. Mon. Wea. Rev., 136, 4882–4898.

[14] Hawkins, J. D., and M. Helveston, 2004: Tropical cyclone multiple eyewall characteristics. Preprints, 26th Conf. on Hurricane and Tropical Meteorology, Miami, FL, American Meteorological Society, P1.7.

[15] Hawkins, J. D., M. Helveston, T. F. Lee, F. J. Turk, K. Richardson, C. Sampson, J. Kent, and R. Wade, 2006: Tropical cyclone multiple eyewall characteristics. Preprints, 27th Conf. on Hurricane and Tropical Meteorology, Monterey, CA, American Meteorological Society, 6B.1.

[16] Hawkins, J. D., and M. Helveston, 2008: Tropical cyclone multiple eyewall characteristics. Preprints, 28th Conf. on Hurricanes and Tropical Meteorology, Orlando, FL, American Meteorological Society, 14B.1.

[17] McNoldy, B. D., 2004: Triple eyewall in Hurricane Juliette. Bull. Am. Meteor. Soc., 85, 1663–1666.

[18] Chen, T. C., S. Y. Wang, and M. C. Yen, 2006: Interannual variation of tropical cyclone activity over the western North Pacific. J. Climate, 19, 5709–5720.

[19] Chia, H.-H., and C. F. Ropelewski, 2002: The interannual variability in the genesis location of tropical cyclones and the northwest Pacific. J. Climate, 15, 2934–2944.

[20] Camargo, S. J., K. A. Emanuel, and A. H. Sobel, 2007: Use of a genesis potential index to diagnose ENSO effects on tropical cyclone genesis. J. Climate, 20, 4819–4834.

[21] Wang, B., and J. C. L. Chan, 2002: How strong ENSO events affect tropical storm activity over the western North Pacific. J. Climate, 15, 1643–1658.

[22] Li, R. C. Y., and W. Zhou, 2012: Changes in western Pacific tropical cyclones associated with the El Niño–Southern Oscillation cycle. J. Climate, 25, 5864–5878.

[23] Gray, W. M., 1984: Atlantic seasonal hurricane frequency. Part I: El Niño and 30-mb quasi-biennial oscillation influences. Mon. Wea. Rev., 112, 1649–1668.

[24] Chu, P.-S., 2004: ENSO and tropical cyclone activity. Hurricanes and Typhoons, Past, Present and Future, R. J. Murnane and K.-B. Liu, Eds., Columbia University Press, New York, pp. 297–332.

[25] Neelin, J. D., C. Chou, and H. Su, 2003: Tropical drought regions in global warming and El Niño teleconnections, Geophys. Res. Lett., 30 (24), 2275.

[26] Yang, Y.-T.,H.-C. Kuo, E. A. Hendricks, M. S. Peng, 2013: Structural and intensity changes of concentric eyewall typhoons in the western North Pacific basin. Mon. Wea. Rev., 141, 2632–2648.

[27] Kummerow, C., W. Barnes, T. Kozu, J. Shiue, and J. Simpson, 1998: The Tropical Rainfall Measuring Mission (TRMM) sensor package. J. Atmos. Ocean. Technol., 15, 809–817.

[28] Hawkins, J. D., T. F. Lee, F. J. Turk, C. Sampson, J. Kent, and K. Richardson, 2001: Real-time Internet distribution of satellite products for tropical cyclone reconnaissance. Bull. Am. Meteor. Soc., 82, 567–578.

[29] Poe, G., 1990: Optimum interpolation of imaging microwave radiometer data. IEEE Trans. Geosci. Remote Sens., 28, 800–810.

[30] Yang, Y.-T., E. A. Hendricks, H.-C. Kuo, and Melinda S. Peng, 2014: Long-lived concentric eyewalls in Typhoon Soulik (2013).Mon. Wea. Rev., 142, 3365–3371.

[31] Willoughby, H. E., 1979: Forced secondary circulations in hurricanes. J. Geophys. Res., 84 (C6), 3173–3183.

[32] Rozoff, C. M., W. H. Schubert, and J. P. Kossin, 2008: Some dynamical aspects of hurricane eyewall replacement cycles. Quart. J. R. Meteor. Soc., 134, 583–593.

[33] Kossin, J. P., W. H. Schubert, and M. T. Montgomery, 2000: Unstable interaction between a hurricane's primary eyewall and a secondary ring of enhanced vorticity. J. Atmos. Sci., 57, 3893–3917.

[34] Zhou, X., and B. Wang, 2011: Mechanism of concentric eyewall replacement cycles and associated intensity change. J. Atmos. Sci., 68, 972–988.

[35] DeMaria, M., and J. Kaplan, 1999: An updated Statistical Hurricane Intensity Prediction Scheme (SHIPS) for the Atlantic and eastern North Pacific basins. Wea. Forecasting, 14, 326–337.

[36] Knaff, J. A., C. R. Sampson, and M. DeMaria, 2005: An operational statistical typhoon intensity prediction scheme for the western North Pacific. Wea. Forecasting, 20, 688–699.

[37] Krishnamurthy L., G. A. Vecchi, R. Msadek, H. Murakami, A. Wittenberg, and F. Zeng, 2016: Impact of strong ENSO on regional tropical cyclone activity in a high-resolution climate model in the North Pacific and North Atlantic oceans. J. Climate, 29, 2375–2394.

[38] Yang, Y.-T.,H.-C. Kuo, E. Hendrick, Y.-C. Liu, and M. Peng, 2015: Relationship between typhoons with concentric eyewalls and ENSO in the western North Pacific basin. J. Climate, 28, 3612–3623.

[39] Hendricks, E. A., M. S. Peng, B. Fu, and T. Li, 2010: Quantifying environmental control on tropical cyclone intensity change. Mon. Wea. Rev., 138, 3243–3271.